Photon Diagnostics for the X-ray FELs at TESLA

M. Tischer, P. Ilinski[*], U. Hahn, J. Pflüger, H. Schulte-Schrepping

Hamburger Synchrotronstrahlungslabor HASYLAB, Deutsches Elektronen-Synchrotron DESY,

Notkestr. 85, D-22603 Hamburg, Germany

[*]*Advanced Photon Source, Argonne National Laboratory, 9700 S. Cass Ave., Argonne, IL 60439, USA*

Abstract

An X-ray diagnostic station will be installed for each of the XFEL undulator beamlines at TESLA. Primary purpose of the X-ray diagnostics is to provide an additional tool for alignment and commissioning of the numerous undulator cells along an XFEL beamline independently from electron beam based alignment procedures. Both methods will complement one another. The X-ray diagnostic station will be a sensitive instrument generating essential input for the undulator control system. The diagnostic station will be located about 120 m downstream from the last undulator cell. Total flux measurements will verify the XFEL's gain. Analysis of the spectral and spatial distribution of the spontaneous radiation of individual or several consecutive undulator segments will be used to optimize angle and position of the electron beam trajectory, to verify the magnetic gap, and to adjust the phase match between two undulator segments. The two latter purposes cannot be served by electron beam based alignment.

TESLA–FEL   2000 – 13

August 2001

1 Introduction

The FEL laboratory at TESLA will provide ten undulator beamlines, five of them will be SASE undulators, the others spontaneous devices. The overall project is defined in the TESLA Technical Design Report (TDR) [1], a general layout of the undulator systems can be found in Section 4.3. of the TDR. The primary SASE undulators are four planar devices operating in the energy range from 2.5 keV to 14.6 keV. SASE5 is a secondary undulator with variable elliptical polarization in the 0.2 keV to 3 keV region. The spontaneous undulators will cover the hard X-ray region up to 450 keV.

The TESLA undulator systems are subdivided into short cells of 6.1 m length. Each undulator cell consists of a variable gap undulator segment of 5 m length and a 1.1 m long intersection module containing various items such as a phase shifter, a quadrupole with an integrated BPM, steering coils, and vacuum components. Gap motion and gap dependent settings of phase shifter, steerers, etc. will be managed within each cell by a local control system which is part of a central undulator control unit.

A single undulator system may have between 10 and 53 segments. All segments and inter-sections of an undulator system will be installed and surveyed by conventional means with a precision of about 300 µm. However, to drive the SASE process into saturation, the overlap between electron beam and radiation field has to be on a ~10 µm scale along the entire undulator, i.e. the individual trajectories through the various undulator segments have to be aligned with this precision.
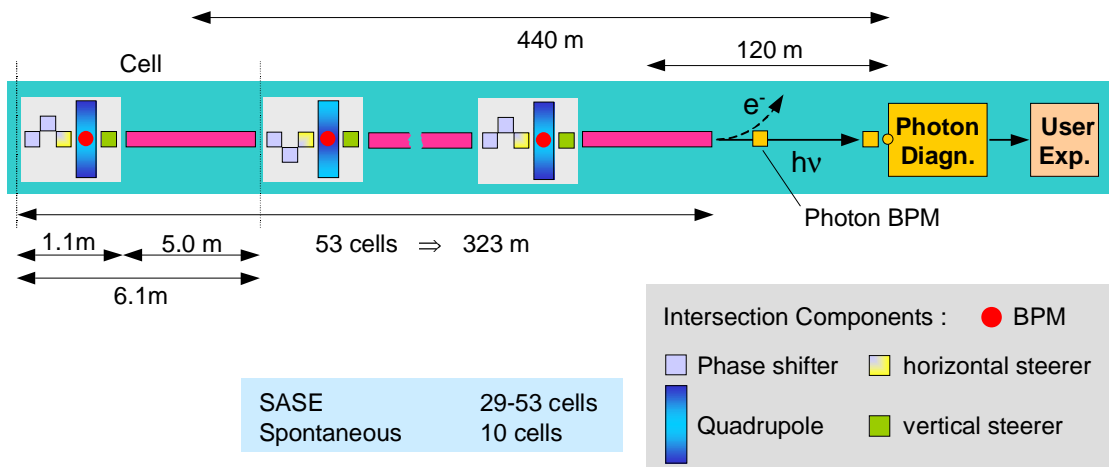

Fig. 1: Schematic outline of the TESLA FEL beamline SASE1. A single diagnostic station is foreseen for up to ~50 cells of an undulator system. Properties of a specific cell can be measured by switching off (i.e. opening gap) of all other segments.

The X-ray diagnostic station is a tool for photon beam based alignment and allows to characterize the radiation of an entire undulator system or individual segments. Each of the ten undulators is equipped with such a system illustrated in Fig. 1. As all undulators will be equipped with a gap drive individual segments can be selected for diagnosis by switching off, i.e. opening the gap of all other segments. This concept of only one common diagnostics for all (~50) undulator cells avoids a multiple installation of identical diagnostic devices which all would have to be calibrated against each other. It rather facilitates a precise alignment and setup of the whole undulator system.

First step in the setup procedure is an alignment of the individual trajectory within each undulator cell. The center of the spontaneous synchrotron radiation cone will be recorded and matched onto a reference point by means of steering coils in the intersection module upstream of the specific undulator segment. Two BPMs in the diagnostic station serve to distinguish an angular misalignment from a transversal offset. Once the trajectories of all segments lie on the same axis, the gap, i.e. photon energy, of each segment can be proven with respect to a selected monochromator energy by maximizing the radiation intensity. Finally, the phase match of successive cells can be optimized by monitoring the photon intensity as function of the phase shift in the intermediate intersection.

Electron beam based alignment which is commonly used to align quadrupole axes is also an appropriate tool to match undulator trajectories [2-4]. Primary purpose of the X-ray diagnostics is to have an additional tool for alignment and commissioning of the numerous undulator cells along a XFEL beamline independently from the electron beam based align-ment procedure. Both methods will complement one another as the latter gives no insight into the magnetic gap or the phase match of adjacent undulator segments.

Photon diagnostics has successfully been used for the TESLA Test Facility TTF [5] and the LEUTL FEL [6], and has been proposed for the LCLS project [7]; preliminary ideas have also been proposed for the TESLA undulators [8]. The main difference to the TESLA FEL project is the gap tunability of the undulators. This enables to place a single diagnostic device at the end of the undulator system as all segments can be switched off individually but on the other hand additionally requires to characterize and control the gap and the phase advance of adjacent segments.

This report discusses the X-ray diagnostics for undulator system SASE1 as a prototype representative for all beamlines. It is operating in an energy range from 2.5 keV to 12.4 keV. As both SASE and spontaneous undulators are multiple segmented devices there will be no general difference in terms of diagnostic issues or the necessity for alignment though the optics has to be adapted for the individual beamlines. Only SASE5 as a helical soft X-ray device needs a different diagnostics concept.

2 Diagnostic Issues

The various alignment aspects all aim at a maximum overlap between electron beam and radiation field. In order to make this a relevant and meaningful task the electron beam has to be sufficiently stable. Besides the specified emittance of 1.6 mrad mm, a position and pointing stability have to be guaranteed better than 10% of the nominal source size and divergence from pulse to pulse (i) at the undulator entrance, i.e.

$$\Delta\sigma_e^{(i)} < 0.1\ \sigma_e \quad \text{and} \quad \Delta\sigma_e^{(i)\prime} < 0.1\ \sigma_e' \,.$$

The requirement to the electron energy stability is even stronger as it contributes quadratically to the radiation wavelength.

The electron pulses with a length of ~1 ms consist of about 11000 individual bunches and have a repetition rate of 5 Hz. Possibly the first bunches of each pulse have to be omitted as they will be used by a fast feedback system to stabilize the remaining bunch. The diagnostics will operate by analyzing the radiation of a single pulse. Depending on the electron beam stability a series of measurements has to be done to determine average properties.

There are three major diagnostic issues which relate to the proper setup of the undulator cells:

    i) Trajectory alignment
    ii) Gap adjustment
    iii) Phase tuning

i) Trajectory alignment. The FEL process is very sensitive to any deterioration of the overlap of electron beam and radiation field. It has been shown [9] that an rms-value of 7 µm along the entire undulator is an upper limit for the orbit deviation. The main contribution to that arises from random trajectory offsets at the quadrupole locations. A random rms quadrupole offset of 1 µm will lead to a gain reduction of ~10%. According to that, an orbit displacement by 1 µm, corresponding to a 2nd field integral of $I_2 = 83$ Tmm^2 , is considered as upper limit for the trajectory displacement within a single undulator segment. Consequently, the angular alignment of the trajectory within a 5 m long undulator segment has to be smaller than 0.2 µrad.

Trajectory alignment implies the horizontal and vertical adjustment of both the trajectory position and also the tilt angle. However, having only one diagnostic station at the end of the undulator system creates an ambiguity in the interpretation of an observed off-axis radiation pattern. Therefore two photon BPMs installed in the drift space between undulator exit and the diagnostic station have to provide the distinction between a trajectory shift and tilt which may result in a radiation spot observed at the same point of the detector. The photon BPMs need a resolution of about 1 µm.

ii) Gap adjustment. Radiation properties like spectral bandwidth or power growth rate are determined by the Pierce parameter ρ which is a fundamental quantity in FEL theory. In the short wavelength regime of SASE1 the ρ-parameter is about $4 \cdot 10^{-4}$. ρ is also a natural measure for some accuracy requirements of the undulator magnetic field, e.g. the averaged peak field value within an undulator segment.

In contrast to the FEL at the TESLA Test Facility (TTF), all TESLA undulators will be variable gap devices. The magnetic peak field as function of the gap will be characterized with an accuracy $< 10^{-4}$ to calibrate the gap separation drive [10,11]. Nevertheless it is essential to have a tool for direct measurement of the energy spectrum of the undulator radiation during operation.

iii) Phase tuning. Changing the undulator gap will result in a change of the phase relation between two adjacent segments. In order to compensate the wavelength dependent phasing condition, a phase shifter is installed in the intersection module [12]. It consists of a three-magnet chicane which is powered by a gap dependent current, and delays the electron beam so that the radiation from the following segment is in phase with that of the previous for all wavelengths.

Requirements on phase tuning are comparatively relaxed. The adjustment of the optical phase has to be assured, i.e. controlled and monitored, with an accuracy of only ~1% or a few degrees [13].

Further radiation properties will be analyzed in order to characterize the FEL performance:
    iv) Integral power
    v) SASE gain
    vi) Emittance measurement

iv) Integral power. This implies a measurement of the total radiation power integrated over the complete spectrum of one or two spontaneously radiating undulator cells. This device should complement the other diagnostic components.

v) SASE gain. The gain determination of the SASE process is an essential goal as it is the quantity characterizing the overall performance. An additional high heat load optics different to that used for the alignment of the undulator cells (i-iii) is required to measure the power of the SASE beam. It should provide a resolution of several percent of the saturation power.

vi) Emittance measurement. The determination of the electron beam emittance is not a primary diagnostic issue for setting up the undulator cells but characterizes the linac per-formance. Supplemental to an emittance determination by optical transition radiation (OTR) or a wire scanner, it can be calculated from the spatial distribution of the photon beam supposed the beta function is known.

3 Concept

For the purpose of setting up the correct trajectory, we will restrict to the strategy of characterizing the radiation of always one undulator cell at a time (or two successive for the phase tuning approach). Wavefront calculations have been performed for the parameters of SASE1 [14] using SRW [15] in order to predict the properties of the undulator radiation observed at the diagnostic station. As illustrated in Fig. 1 the observation point of the radiation of the individual cells varies by a factor of ~4 along the entire undulator system. The spatial distribution is fully dominated by the angular divergence so that the obtained beam pattern can be scaled according to their distance. The accuracy of the diagnostic station is limited by the finite resolution of the imaging components, and in this respect the characterization of the last undulator segment defines the requirements on the imaging system. For the ease of comparison all calculations have been performed for an observation point 100 m behind the source. In the following the conceptual framework of the three major diagnostic issues is discussed.

i) Trajectory alignment

The fundamental radiation wavelength λ_R of an undulator is given by

$$\lambda_R = \frac{\lambda_u \cdot \left(1 + K_{rms}{}^2 + \gamma^2\left(\theta^2 + \psi^2\right)\right)}{2\gamma^2} \tag{1}$$

where λ_U is the undulator period, K_{rms} the rms undulator parameter, γ is the kinetic energy of the electrons measured in units of its rest mass, and θ and ψ the emission angles of the radiation. While the relative bandwidth $\Delta\lambda/\lambda$ scales with $1/nN$, the angular half-width $\sigma_{r'}$ of the nth harmonic is determined by

$$\sigma_{r'} \cong \frac{1}{\gamma}\sqrt{\frac{1 + K_{rms}^2}{2nN}} \quad . \tag{2}$$

Spontaneous radiation of the 1st, 3rd or 5th harmonic can be used for the different alignment aspects depending on the required accuracy. The top part of Fig. 2 shows the energy spectrum of the 1st harmonics of a single SASE1 undulator segment. For comparison, the dashed and solid curves represent calculations for a filament electron beam and for inclusion of the finite emittance, respectively. As expected, the emittance influence is still small for the (spontaneous) spectrum of the 1st harmonics. The lower part of Fig. 2 displays spatial distributions for slightly different observation energies of the fundamental undulator peak; the 2-dimensional images are intensity distributions which include the broadening due to emittance. The line scan in Fig. 2 b) shows the spatial distribution for an observation energy corresponding to the undulator harmonics. It has an angular half width of ±4 μrad equivalent to the value obtained

by Eq. 2. For a detuning of the observation energy towards lower values, a broadening accompanied by a splitting of the intensity cone towards a ring is obtained. Detuning by ~5‰ to higher energies (Fig. 2 c) leads to a considerable narrowing of the radiation cone, however to the expense of lower intensity.
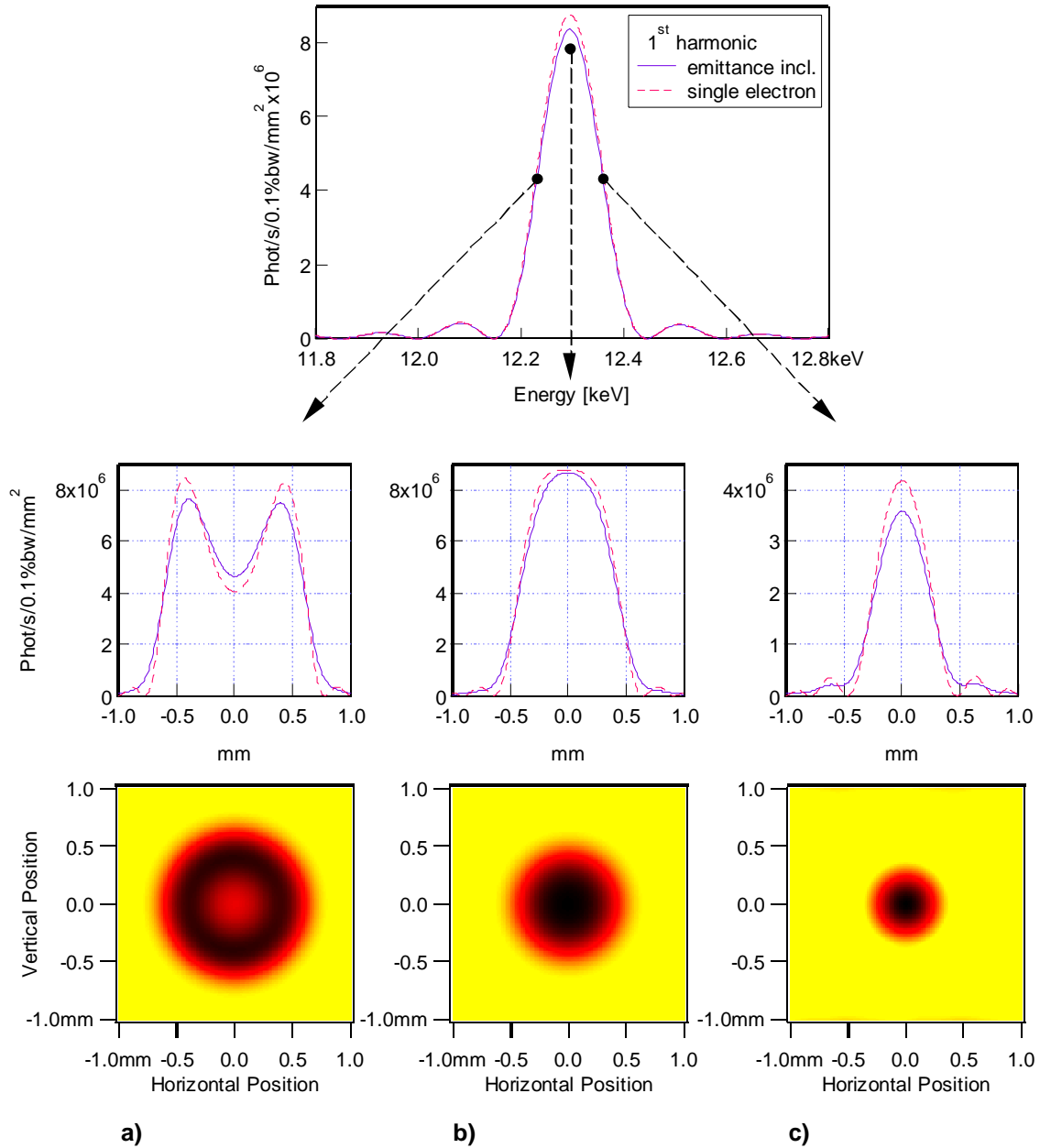

Fig. 2 top part: Energy spectrum of the spontaneous radiation of a single 5 m long undulator segment calculated for the parameters of SASE1 at a wavelength of ~1 Å. The dashed and solid line correspond to a calculation without and with inclusion of emittance effects, respectively, indicating that the spontaneous spectrum at these energies is still dominated by its intrinsic broadening.
lower part a–c): Profile and 2D spatial intensity distribution of the circular beam expected for different observation energies (12.24 keV, 12.30 keV, 12.36 keV) in the vicinity of the undulator peak (arrows) at a distance of 100 m behind the source. (Color bars of the 2D images are not scaled to each other.)

It should be emphasized that the center of gravity for all three intensity distributions in Fig. 2 is on the beam axis independent of observing the radiation on- or off-crest of the undulator spectrum. Therefore, the photon beam axis, and hence the mean undulator trajectory, can be detected independently of a possibly incorrect gap setting.

A still smaller spot size is obtained for higher harmonics of the undulator radiation. Calculations have been performed for several observation energies close to the 3rd and 5th harmonics. Fig. 3 compares the spatial distributions for an observation energy detuned by a few ‰ above the higher harmonics peak. As expected the emittance induced portion of the profile broadening becomes more apparent for higher harmonics when the total line width decreases. A full width at half maximum (FWHM) of 330 µm and 280 µm at a distance of 100 m is obtained for the 3rd and 5th harmonic, respectively. Going to even higher energies narrows the spatial distribution only by a negligible amount (~10µm) as the photon beam divergence is now dominated by the emittance.

The spatial distribution shows a symmetric pattern, and its center of gravity determines the electron trajectory within an undulator segment. Assuming a mean spatial line width of ~330 µm, an accuracy of ~7% of the FWHM (working with the 5th harmonics) or correspondingly 20 µm of the obtained spatial distribution has to be achieved in order to cope with the specified angular resolution of 0.2 µrad. The setup presented in Section 4 will easily meet this requirement. The intensity spectra shown above have been calculated for a single pulse of 1 nC which yields sufficient photons for a single shot measurement. From the last to the 1st undulator segment the flux density at the diagnostic station drops by a factor of ~10. This still provides reasonable statistics for a center of gravity determination of the photon spot.

It is evident that the analysis of the photon spot as a single footprint of the electron trajectory through the undulator cannot distinguish between a shifted and a tilted orbit. The two installed photon BPMs (Fig. 1) are sufficient to resolve this ambiguity (Section 4).
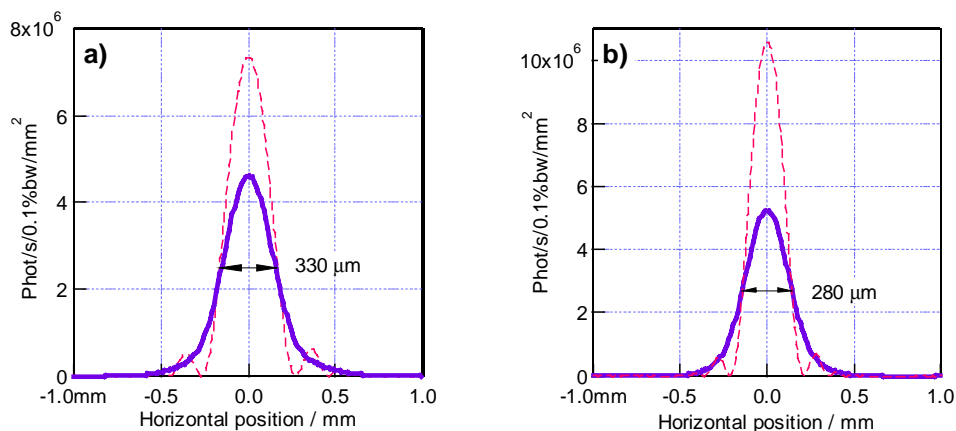

Fig. 3: Intensity profiles of the 3rd (a) and 5th (b) harmonics for parameters and conditions according to Fig. 2 c), i.e. an observation energy detuned slightly above the undulator peak. The spatial distribution narrows considerably with higher energies until broadening due to emittance (taken into account in the blue solid curves) dominates the undulator spectrum.

ii) Gap adjustment

The magnetic gap of an undulator segment can be deduced by scanning over an undulator harmonics. Fig. 4 shows the spontaneous radiation spectrum of the 5th harmonics as function of the energy for three different gap values. The undulator line has a relative band width of $2.2 \cdot 10^{-3}$. Once the trajectories in the different undulator segments are all on the same axis, each gap can be adjusted by two means:

a) An energy spectrum is taken whose center of gravity defines the energy position of the undulator harmonics for the present gap. This has to be adjusted to the nominal value. The uncertainty in the measured fundamental energy has to be smaller than the ρ parameter $(4 \cdot 10^{-4})$, i.e. the undulator harmonics have to be determined with a precision of 18% of the line width.

b) The gap can be optimized by maximizing the intensity at the desired photon energy which is then kept fixed. Corresponding to the ρ parameter for SASE1 the precision requirement for the gap adjustment is in the order of ~3 µm. Fig. 5 displays the intensity obtained for a fixed observation energy corresponding to the 5th harmonics (61.5keV) as function of the gap detuning from its nominal value. It can be seen that the observed intensity varies considerably with a small gap misalignment; an intensity drop of ~8% is expected for a gap deviation of 3 µm. This method will work much faster than the first approach.
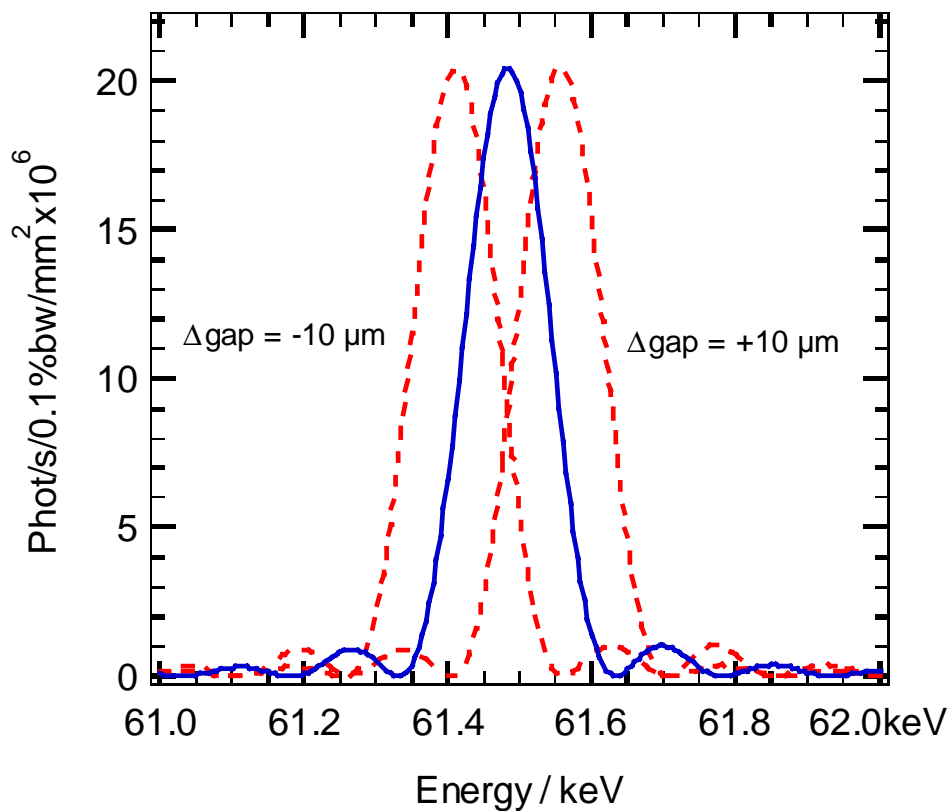

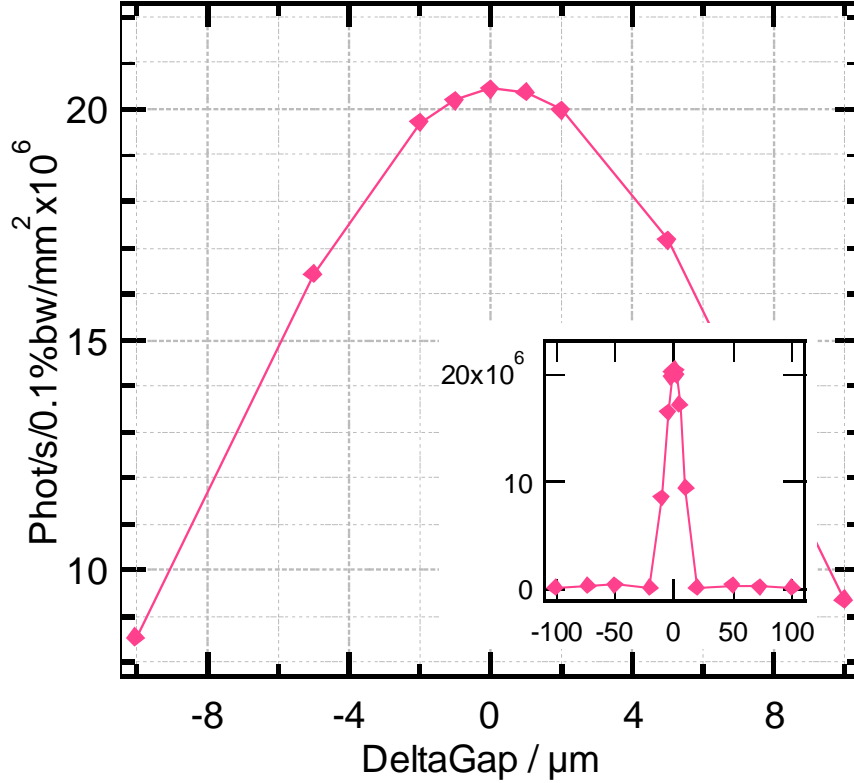**Fig. 4:** Energy spectra of the 5th harmonics for three slightly different gap settings.

Fig. 5: Photon intensity as function of gap detuning for a constant observation energy of 61.5 keV (5th harm.); the reference gap corresponds to the open gap position (23mm).

Gap tuning of all undulator segments in a successive way, i.e. always only one undulator gap is closed, will result in identical fundamental energies of all segments. A taper of the gap along the entire undulator system, which is required to optimize the SASE intensity, has to be fine-adjusted subsequently.

iii) Phase tuning

The phase condition of two adjacent undulator cells radiating at the wavelength λ_R depends on their separation length L. Figure 6 illustrates the field distribution of two successive segments. In this sketch L is the distance between the two endpoles; for simplicity they have full strength but only half length. In a real structure L is considered as the distance between the last full poles. For constructive interference, the phase advance $\Delta\varphi$ has to be a multiple of 2π, and can be written as [12]

$$\Delta\varphi[rad] = 2\pi\eta \qquad \text{with} \qquad \eta = \frac{L}{2\gamma^2\lambda_R} = \frac{L}{\lambda_0\left(1 + K_{rms}^2\right)} \ , \qquad (3)$$

(e.g. L = 1.1 m, λ_R = 1 Å, and E = 25 GeV $\Rightarrow$ η = 2.30)

An additional phase delay $(\nu-\eta)\cdot2\pi$ (ν=1,2,3…) has to be applied to the electron beam by the phase shifter in order to bring the radiation of the two segments to a constructive interference.
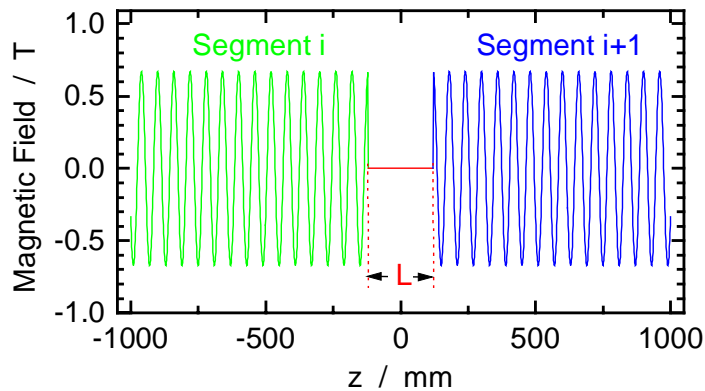
10

Fig. 6: Schematic field distribution of two undulator segments separated by a distance L.

The adjustment of the correct phase is based on the observation of the radiation of two successive undulator segments. The phase relation between them affects the energy spectrum as well as the spatial distribution of the composed radiation (Fig. 7). For complete phase match (red) the undulator line peaks at E_{fund}; the spectrum of a single segment (green) is
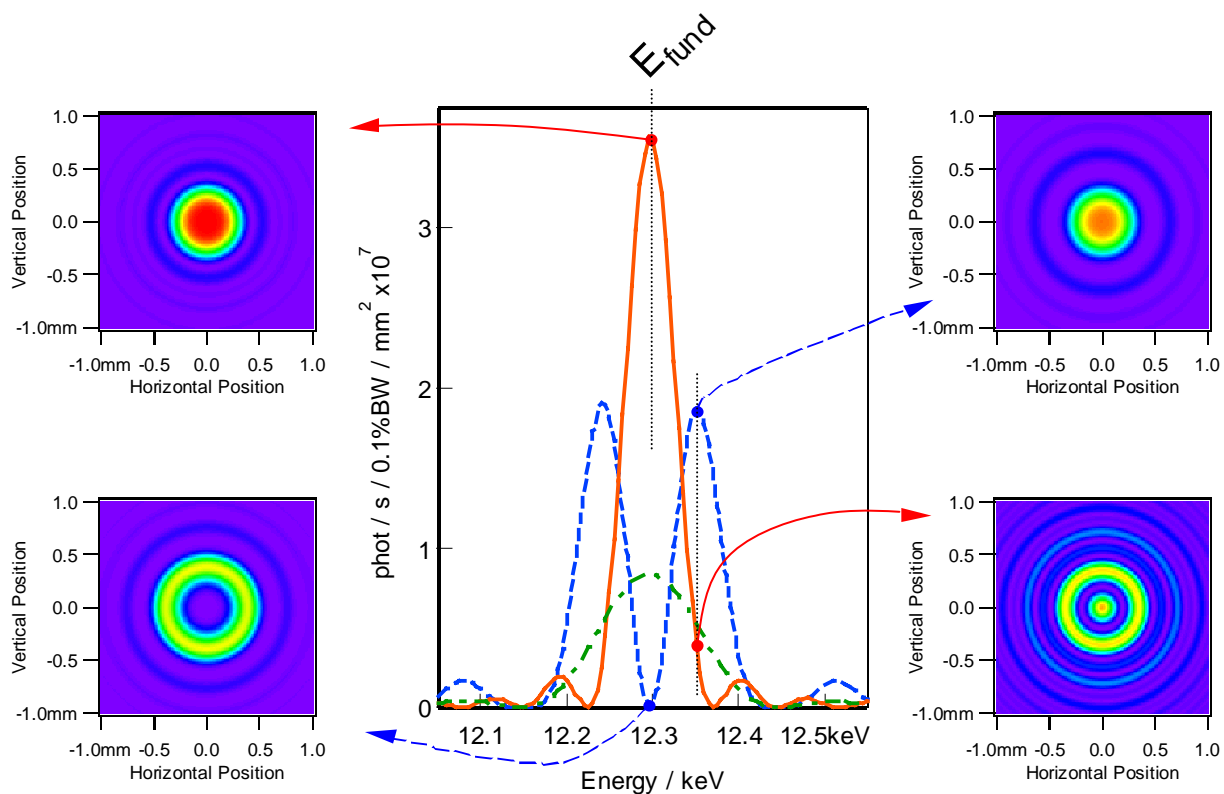

Fig. 7: Spectral distribution of two successive undulator segments – which both have their fundamental energy at 12.295 keV – for a phase difference of 2π (solid red) and π (dashed blue). The corresponding spatial intensity distributions are strongly structured once the detection energy deviates from the undulator fundamental and the phase shift differs from 2π (color bars are not scaled to each other). The spectrum of a single undulator segment is shown for comparison (dash-dot green).

shown for comparison. In case of fully destructive interference (blue), the undulator spectrum shows intensity maxima below and above E_{fund}. The spatial radiation distribution at $E = E_{fund}$ is cone-like in the matched phase condition whereas the radiation is emitted in a ring in the destructively interfering case.

The easiest way to monitor the phase is to observe the photon intensity at constant energy $E_{obs} = E_{fund}$ while shifting the optical phase in the electron chicane. It can be seen from the red line in Fig. 8 that the observed photon flux varies by a factor of ~400 for a phase advance from π to 2π. The intensity oscillates according to ~$1.8 \cdot 10^7 * (1 + \cos(2\pi \varphi))$. Making use of this functional dependence, the optical phase can be tuned within an accuracy of a few degrees. Alternatively, the maximum intensity can be observed at different energies depending on the phase relation (Fig. 7). As seen in Fig. 8 (green) this value varies only by about 50% over one period of the optical phase and thus is less suited to tune the phase advance.
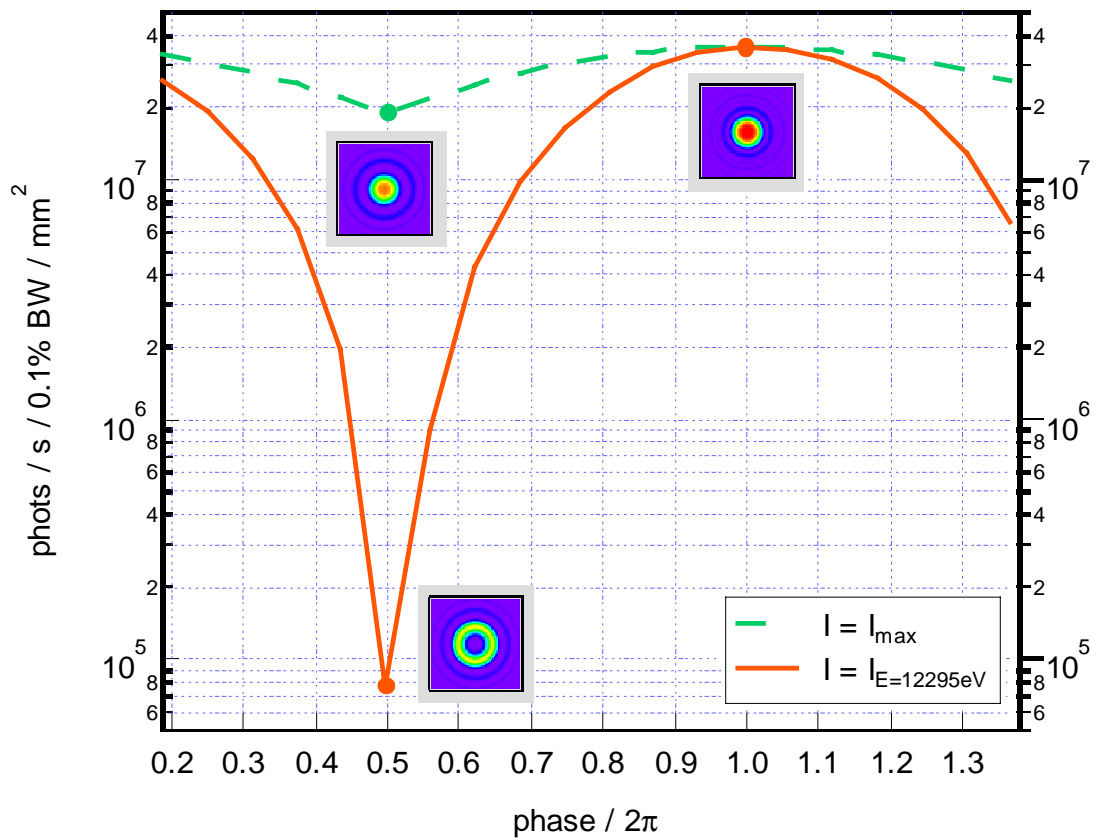

Fig. 8: Expected intensity of two adjacent undulator segments as function of their optical phase (for otherwise identical settings). The dashed green curve shows the maximum intensity of the obtained spectral distribution while the solid red represents the intensity observed at constant energy equivalent to the undulator harmonics; the latter exhibits an intensity variation of ~400 and reveals a sensitive scheme to tune the optical phase.

4 Hardware Setup

The photon diagnostic station can be split up into three parts, i.e. the photon beam position monitors, the central imaging station, and a detector unit for observation of integral properties.

Two photon BPMs will be installed at the beginning and end of the drift section between undulator exit and diagnostic station. They perform a two-fold task: At first, they serve for a coarse trajectory adjustment within the visual field of the imaging setup. Secondly, the monitors will be used in conjunction with the imaging station to precisely align the trajectories of all undulator segments, in particular to distinguish between transversal and angular displacement. Position-sensitive ionization chambers are present state-of the-art photon monitors in terms of resolution and are most appropriate for this application as they do not directly interact with the beam. Ionization chambers with so-called backgammon electrodes, which have been developed at Spring8 [16], exhibit a sensitivity of about 1 µm and are ideally suited for our purposes. Trajectories can be determined with a relative precision of ~2 µm or ~0.02 µrad. Unlike counting detectors, a ionization chamber is charge sensitive and integrates
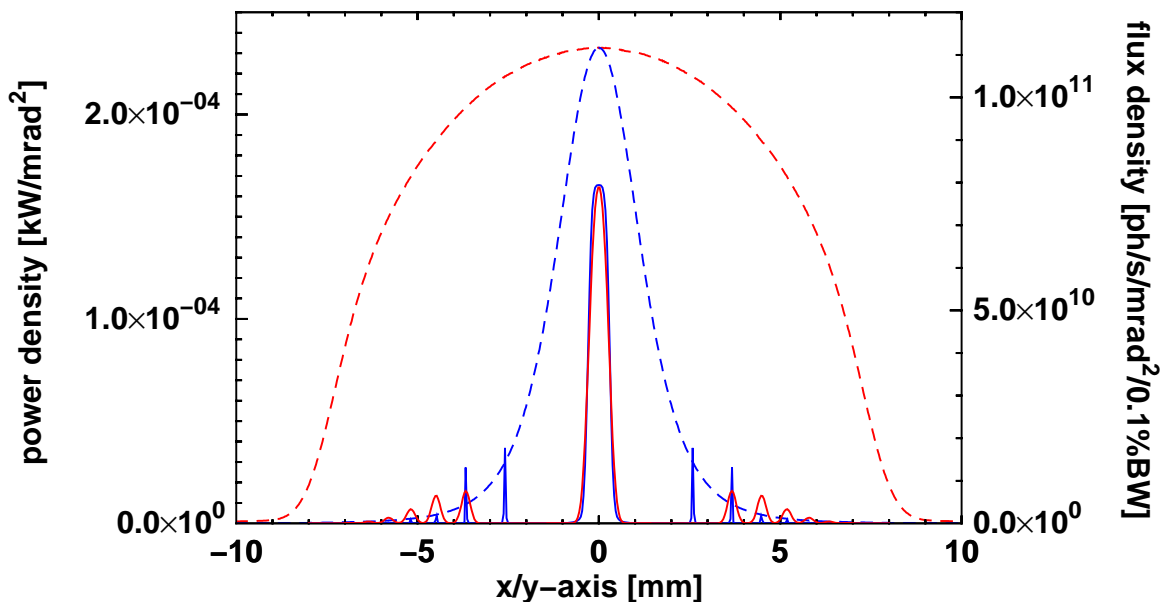

Fig. 9: Calculated power density (dashed) and flux density at the 5th harmonic at 61.5 keV (solid) at a distance of 100 m. Shown are scans through the origin along the horizontal (red) and vertical direction (blue). At an electron current of 1 nA, $3.5 \cdot 10^6$ photons/s/0.1%BW will fall into the central cone.

over the high peak flux. In contrast to the imaging setup which cannot remain in the beam during a user experiment, the photon BPMs will monitor the photon beam continuously.

The primary part of the photon diagnostic station will image the central cone of the mono-chromatized undulator beam of one or several undulator segments. It will be possible to observe an image at the energy of the 1st and 5th harmonic of the XFEL undulator through two different viewports. Due to a reduced beam pipe aperture (~10 mm) at short differentially pumped sections of the beamline, the photon diagnostic station will cover a solid angle of ~80×80 µrad^2 with respect to the last and ~20×20 µrad^2 with respect to the first undulator segment, the latter corresponding to about $(10 \cdot \sigma'_{ph})^2$ in case of the 5th harmonics. Fig. 9 shows the spatial radiation distribution of the 5th harmonics. A field of view with 5 mm diameter is free of additional rings of the same energy as the central cone. This is sufficient to determine FWHM and shape of the central cone. The footprint of the beam as given by the power density profile in the figure is much larger and will be cut off by apertures.

The undulator beam will be monochromatized using a single crystal Laue-case setup similar to that used at the PETRA-undulator beamline at HASYLAB as shown in Fig. 10. There will be two fixed viewports in order to observe the 1st and 5th harmonic of the undulator by only rotating the crystal angle. The observation of two angles allows the determination of an absolute energy scale.

Experience with a similar setup at the undulator beamline [17] of the PETRA storage ring at DESY running with 12 GeV positrons, shows that the images obtained by a single crystal Bragg-case monochromator are not usable for evaluation due to scattered photons from the bulk crystal volume. At PETRA, the hard X-ray background extends up to 500 keV, in the XFEL case due to the higher electron energy of 25 GeV up to several MeV photon energy. A thin Laue-case crystal with a thickness of 200 µm was used successfully at PETRA to image the central cone of the undulator, providing a clear picture without additional spots and high energy background. The Laue-case setup is favorable due to the small Bragg angles of 5.49° and 9.17° required for the 5th harmonic using Si(333) and for the 1st harmonic with Si(111), respectively. The method of using a fluorescent screen and optical imaging this screen with a lens and a CCD camera as shown in Fig. 11 provides a high degree of freedom in terms of imaging ratio and resolution.

Compared to the fibre optic setup the lens method requires additional degrees of freedom for adjusting all parts relative to each other. The optical transmission of the lens system will be in the 5% region, while a fibre optical coupled system yields a transmission of up to 70%. Therefore a system is proposed composed out of a Laue-case crystal monochromatizing the central cone and projecting it onto a fluorescent screen attached directly onto a fibre optic taper. The fluorescent screen will be either directly coated onto the fibre or be a thin film screen attached to the fibre. This taper is part of a fibre optic vacuum window. At the air side of this window a CCD chip will be directly bonded onto the fibre.

Assuming a field of view of 5 mm^2 and the need for a 12 µm^2 CCD pixel size (16 bit reso-lution requires at least a corresponding number of stored electrons in a single pixel area), a

taper with an imaging ratio of 1:2.4 (screen side : CCD side) will be installed. The overall resolution of the system using a 1024×1024 pixel CCD chip will be 5 µm^2/pixel. This estimate assumes present day fibre optic tapers with a fibre diameter of 6 µm at the CCD side. A CCD chip with a higher pixel count usually has a larger pixel size and will not give a higher resolution, but will provide a larger field of view. An option will be replacing the fluorescent screen coating at the fibre end by a doping of the fibre end.
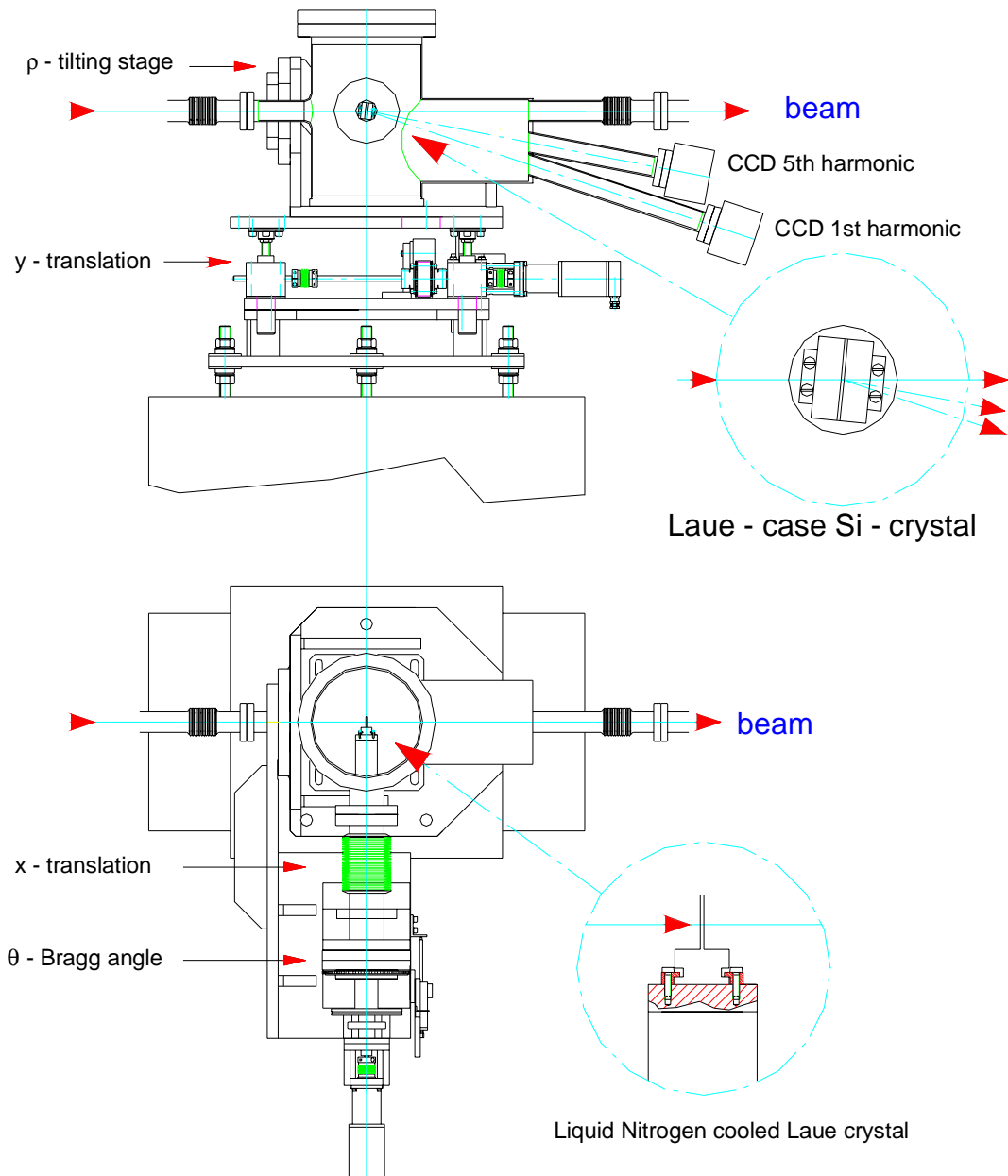

Fig. 10: Schematic view of the diagnostic station setup. A Laue-case silicon crystal monochromatizes the undulator radiation. The central cone will be observed at two photon energies (1st and 5th harmonic) at the corresponding crystal angle setting through fibre optic viewports coated with fluorescent screens. At the air side of the viewports CCD cameras record the images.
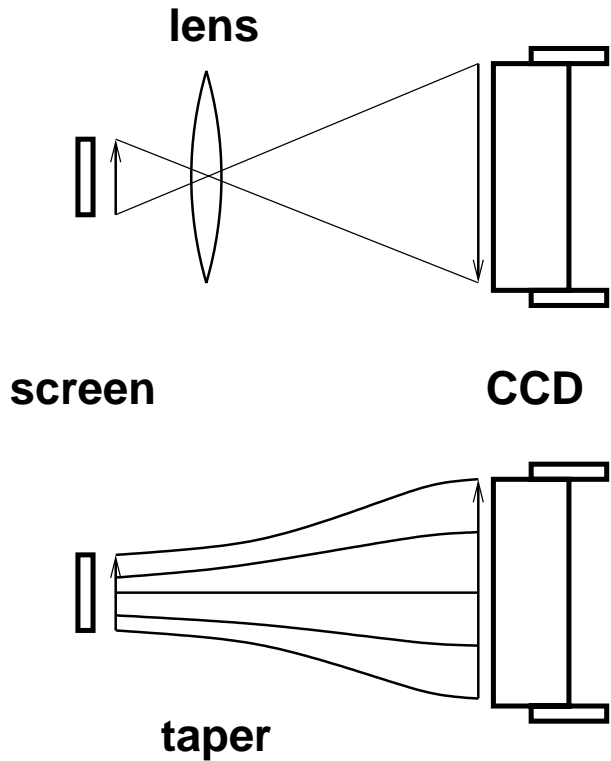
Fig. 11: Sketch comparing the imaging setup using an optical relay lens or a fibre optic taper to transfer the fluorescent screen image to the CCD.

Present day 16 bit resolution CCD systems are driven with a maximum pixel clock of 50 kHz, due to an increase in readout noise at higher clock rates. The dark current in a cooled CCD system is negligible at exposure times in the seconds range. Under these conditions, the setup will be able to provide an image every 20 seconds. A 12 bit system would provide an image in one second or faster, but the dynamic range is too limited to observe the effect of phasing of two undulator segments without changing the exposure time. From our simulations with SRW, we observe a difference in intensity by a factor of 400 while changing the operating conditions from an anti- to a phased mode.

Integral beam properties will be determined in a second station similar to the imaging station (Fig. 10) described above. The integral power of the spontaneous radiation will be measured with either a pin diode or a calorimeter put into the direct beam. The incident power ranges from about 1 mW (47 mW) for a single pulse to 50 W (2.7 kW) for continuous operation in case of a single (all) undulator segment(s) switched on. For determination of the SASE gain and the spectrum a thin diamond crystal in Laue geometry will monochromatize the SASE line. The power in this line will again be measured with either a pin diode or a calorimeter depending on the gain regime of the FEL. The pin diode in the direct beam will then measure the power of the complementary part of the photon spectrum, i.e. the overall background of the SASE line.

5 Conclusions

The basic idea behind the photon diagnostics concept described here is to use one common assembly for all undulator cells within one beamline branch. The main advantage of such a scheme is the realization of identical experimental conditions – except for simple geometrical variations. This makes the measurements of the various segments directly comparable and eases the interpretation of the obtained results considerably. This scheme depends on the gap drive of the undulator segments that allows to turn on and off single segments individually. The alternative concept is to install an optical diagnostic block after each undulator segment; this approach has successfully been realized at the LEUTL SASE FEL [6] working in the visible. The commissioning phase of TTF [5] and LEUTL have clearly demonstrated the necessity and benefit of photon diagnostics.

A common X-ray diagnostic station avoids installation and maintenance of many identical components which all have to be calibrated against each other. The space requirement for multiple diagnostic stations is critical as this additional separation length between adjacent undulators increases the debunching of electrons which is less tolerable in the XFEL regime.

References

[1]   TESLA Technical Design Report Part V, Eds.: G. Materlik, T. Tschentscher, TESLA-FEL 2001-05, DESY (2001)

[2]   "Beam Based Alignment of the TESLA X-ray FEL undulators", B. Faatz, TESLA-FEL 2001-04, DESY (2001)

[3]   "TTF FEL Beam-based Alignment by Dispersion Correction Using Micado Algorithm", P. Castro, TESLA-FEL 1997-04, DESY (1997)

[4]   "Electron Phase Slip in an Undulator with Dipole Field and BPM Errors", P. Emma, LCLS Technical Notes 00-14, SLAC (2000)

[5] "Development of Photon Beam Diagnostics for VUV Radiation from a SASE FEL", R. Treusch, T. Lokajczyk, W. Xu, U. Jastrow, U. Hahn, L. Bittner, J. Feldhaus, Nucl. Instr. Meth. A 445, 456 (2000)

[6] "The magnetic and diagnostics systems for the Advanced Photon Source self-amplified spontaneously emitting FEL", E. Gluskin et al., Nucl. Instr. Meth. A 429, 358 (1999); "Observation of Self-Amplified Spontaneous Emission and Exponential Growth at 530 nm", S. V. Milton for the LEUTL collaboration, Phys. Rev. Lett. 85, 988 (2000)

[7] "Predicted Performance of the LCLS X-ray Diagnostics", E. Gluskin, P. Ilinski, N. Vinokurov, LCLS Technical Notes 00-13, SLAC (2000)

[8] "Design Considerations for a 1 Å SASE Undulator", P. Elleaume, J. Chavanne, B. Faatz, Nucl. Instr. Meth. A 455, 503 (2000); TESLA-FEL 2000-16

[9] "Field Accuracy Requirements for the Undulator Systems of the X-ray FELs at TESLA", B. Faatz, J. Pflüger, TESLA-FEL 2000-14, DESY (2000)

[10] "A Prototype Gap Separation System for the TESLA Undulator", M. Rüter, J. Pflüger, TESLA-FEL 2000-07

[11] "Ein SIMATIC basiertes Kontrollsystem für die Undulatoren des TESLA Röntgen-lasers", H.H. Radszuweit, J. Krunkowski, J. Pflüger, M. Tischer, TESLA-FEL 2000-09, in German

[12] "A Prototype Phase Shifter for the Undulator Systems at the TESLA X-ray FEL", J. Pflüger, M. Tischer, TESLA-FEL 2000-08

[13] B. Faatz, priv. commun.

[14] For all presented calculations of photon spectra, the following parameters have been used according to the specifications for SASE1: $E_e = 25$ GeV, $I_e = 1$ nA, $\varepsilon_n = 1.6$ mrad mm, $\beta = 45$ m, $\Delta E_e/E_e = 10^{-4}$, $\lambda_U = 60$ mm, N = 83 periods, $B_0 = 0.67$ T or $K_{rms} = K_{max}/\sqrt{2} = 2.65$.

[15] SRW, Version 3.7, ESRF 1997-2000, Authors: O. Chubar, P. Elleaume

[16] "Development of a Position Sensitive Ionization Chamber with Backgammon Elec-trodes as a Beam Position Monitor for SR Experiments", K. Sato, T. Kudo, M. Suzuki, T. Ishikawa, Spring8 Annual Report p.181 (1998); "The Position-Sensitive Ionization Chamber for Synchrotron Radiation Experiments", K. Sato, H. Tanida, S. Adachi, Proc. SPIE 3774, 114 (1999)

[17] U. Hahn, H. Schulte-Schrepping, to be published